nature geoscience
SUPPLEMENTARY INFORMATION
https://doi.org/10.1038/s41561-018-0110-z
In the format provided by the authors and unedited.

Indian Ocean floor deformation induced by the Reunion plume rather than the Tibetan Plateau

G. Iaffaldano[1]*, D. R. Davies[2] and C. DeMets[3]

[1]Department of Geosciences and Natural Resource Management, University of Copenhagen, Copenhagen, Denmark. [2]Research School of Earth Sciences, The Australian National University, Canberra, Australia. [3]Department of Geoscience, University of Wisconsin-Madison, Madison, WI, USA.
*e-mail: giia@ign.ku.dk

Indian Ocean Floor Deformation Induced by the Reunion Plume rather than the Tibetan Plateau

G. Iaffaldano[1], D. R. Davies[2], and C. DeMets[3]

[1]Department of Geosciences and Natural Resource Management, University of Copenhagen – Denmark.
[2]Research School of Earth Sciences, The Australian National University – Canberra, Australia.
[3]Department of Geoscience, University of Wisconsin–Madison – Wisconsin, USA.

Supplementary Tables and Figures

Supplementary Table 1: REDBACK parameters used for noise mitigation on the finite rotations of *Bull et al.* [1] that reconstruct the past position of SO relative to CP.

Parameter	Value	Units
`ensemble_size`	$2 \cdot 10^7$	Dimensionless
`burn_in`	10^4	Dimensionless
`max_partitions`	20	Dimensionless
`time_sigma`	1	Myr
`lon_sigma`	1	$^\circ$
`lat_sigma`	0.1	$^\circ$
`ang_sigma`	0.1	$^\circ$
`lon_sigma_bd`	1	$^\circ$
`lat_sigma_bd`	0.1	$^\circ$
`ang_sigma_bd`	0.1	$^\circ$
`hp_lon_min`	0.1	Dimensionless
`hp_lon_max`	10	Dimensionless
`hp_lon_sigma`	0.5	Dimensionless
`hp_lat_min`	0.1	Dimensionless
`hp_lat_max`	15	Dimensionless
`hp_lat_sigma`	1	Dimensionless
`hp_ang_min`	0.1	Dimensionless
`hp_ang_max`	10	Dimensionless
`hp_ang_sigma`	0.2	Dimensionless

Supplementary Table 2: REDBACK parameters used for noise mitigation on the finite rotations of *Bull et al.* [1] that reconstruct the past position of SO relative to IN.

Parameter	Value	Units
`ensemble_size`	$2 \cdot 10^7$	Dimensionless
`burn_in`	10^4	Dimensionless
`max_partitions`	20	Dimensionless
`time_sigma`	1	Myr
`lon_sigma`	0.7	$^\circ$
`lat_sigma`	1	$^\circ$
`ang_sigma`	0.005	$^\circ$
`lon_sigma_bd`	0.7	$^\circ$
`lat_sigma_bd`	1	$^\circ$
`ang_sigma_bd`	0.005	$^\circ$
`hp_lon_min`	0.1	Dimensionless
`hp_lon_max`	10	Dimensionless
`hp_lon_sigma`	0.2	Dimensionless
`hp_lat_min`	0.1	Dimensionless
`hp_lat_max`	10	Dimensionless
`hp_lat_sigma`	1	Dimensionless
`hp_ang_min`	0.1	Dimensionless
`hp_ang_max`	10	Dimensionless
`hp_ang_sigma`	0.2	Dimensionless

Supplementary Table 3: Stage Euler vectors for the motion of CP relative to fixed SO, following noise mitigation through the REDBACK software. Axes x, y and z of the Cartesian reference frame correspond to (0°E, 0°N), (90°E, 0°N), and (90°N), respectively. Covariance matrices are symmetric, thus only upper triangles are tabulated.

Young age	Old age	ω_x	ω_y	ω_z	c_{xx}	c_{xy}	c_{xz}	c_{yy}	c_{yz}	c_{zz}
$[Ma]$		$[10^{-1}\ ^\circ/Myr]$			$[10^{-8}\ rad^2/Myr^2]$					
0	0.781	3.95	4.75	1.27	24	24	8	35	7	8
0.781	1.778	3.94	4.67	1.27	12	12	4	17	3	5
1.778	2.581	3.96	4.59	1.30	12	11	4	17	3	5
2.581	3.596	3.97	4.51	1.34	17	16	5	23	4	5
3.596	5.235	4.02	4.41	1.41	16	15	5	20	4	5
5.235	6.033	3.75	3.96	1.37	36	38	12	46	12	7
6.033	6.733	3.63	3.75	1.36	40	42	13	50	14	7
6.733	8.132	3.47	3.45	1.35	43	46	15	53	16	7
8.132	9.105	3.54	3.40	1.41	75	80	26	92	28	12
9.105	9.786	3.55	3.33	1.44	62	63	21	72	23	11
9.786	11.067	3.54	3.23	1.47	37	37	13	42	13	7
11.067	12.464	3.64	3.21	1.56	34	32	12	37	12	7
12.464	14.607	3.80	3.21	1.68	24	22	8	25	8	6
14.607	15.974	4.17	3.42	1.89	61	58	22	62	22	13
15.974	17.235	4.20	3.31	1.94	56	50	20	55	20	13
17.235	18.056	4.33	3.34	2.03	127	115	48	121	46	26
18.056	19.722	3.96	2.84	1.92	100	80	36	94	34	24

Supplementary Table 4: Stage Euler vectors for the motion of IN relative to fixed SO, following noise mitigation through the REDBACK software. Axes x, y and z of the Cartesian reference frame correspond to (0°E, 0°N), (90°E, 0°N), and (90°N), respectively. Covariance matrices are symmetric, thus only upper triangles are tabulated.

Young age	Old age	ω_x	ω_y	ω_z	c_{xx}	c_{xy}	c_{xz}	c_{yy}	c_{yz}	c_{zz}
$[Ma]$		$[10^{-1}\ ^\circ/Myr]$			$[10^{-8}\ rad^2/Myr^2]$					
0	0.781	3.24	2.08	1.42	25	15	10	12	6	7
0.781	1.778	3.23	2.06	1.43	12	6	4	6	2	4
1.778	2.581	3.25	2.05	1.47	16	9	6	8	3	6
2.581	3.596	3.32	2.06	1.53	53	32	23	24	14	14
3.596	5.235	3.07	1.84	1.49	21	12	9	10	5	6
5.235	6.033	3.02	1.76	1.51	43	24	18	19	11	12
6.033	6.733	3.17	1.84	1.61	38	21	16	18	9	12
6.733	8.132	3.11	1.76	1.63	9	4	3	6	1	4
8.132	9.105	3.07	1.69	1.67	13	5	5	9	1	7
9.105	9.786	3.03	1.64	1.68	20	9	9	12	3	9
9.786	11.067	3.06	1.62	1.73	11	4	4	9	0	6
11.067	12.464	3.11	1.64	1.80	7	1	3	8	-1	5
12.464	14.607	3.15	1.72	1.84	8	2	4	9	-1	6
14.607	15.974	3.53	2.11	2.05	36	15	17	22	6	14
15.974	17.235	4.20	2.63	2.41	84	37	41	48	18	29
17.235	18.056	4.03	2.59	2.34	88	31	41	62	13	35
18.056	19.722	3.50	2.34	2.08	120	31	48	99	10	64

Supplementary Table 5: Finite rotations that reconstruct the past position of SO relative to CP, following noise mitigation through the REDBACK software. Axes x, y and z of the Cartesian reference frame correspond to (0°E, 0°N), (90°E, 0°N), and (90°N), respectively. Covariance matrices are symmetric, thus only upper triangles are tabulated. The finite rotation at 8.132 Ma has been bootstrapped from the noisy data set and interpolated in the noise–mitigated series.

Age [Ma]	Lon. [°E]	Lat. [°N]	Angle [° CCW]	c_{xx}	c_{xy}	c_{xz}	c_{yy} [10^{-8} rad^2]	c_{yz}	c_{zz}
0	50.28	11.68	0.02	9	11	17	13	20	31
0.781	50.27	11.59	0.51	11	10	12	11	17	28
1.778	50.04	11.68	1.14	22	16	16	18	26	47
2.581	49.81	11.82	1.63	36	25	23	27	40	71
3.596	49.48	12.04	2.26	60	41	39	44	65	116
5.235	48.93	12.43	3.26	112	75	71	80	117	208
6.033	48.65	12.64	3.71	129	81	69	85	123	223
6.733	48.41	12.83	4.09	145	87	70	90	130	238
8.132	47.89	13.23	4.80	180	104	81	108	154	281
9.105	47.53	13.51	5.29	164	76	32	75	105	212
9.786	47.28	13.71	5.64	170	75	26	74	103	210
11.067	46.80	14.08	6.28	177	72	16	70	98	204
12.464	46.28	14.49	6.98	194	79	23	78	109	222
14.607	45.48	15.13	8.10	216	95	44	94	132	252
15.974	44.98	15.54	8.88	181	61	1	60	85	180
17.235	44.52	15.91	9.59	177	60	3	60	84	175
18.056	44.22	16.15	10.06	206	87	42	87	122	226
19.722	43.60	16.65	10.92	220	82	26	83	117	224

Supplementary Table 6: Finite rotations that reconstruct the past position of SO relative to IN, following noise mitigation through the REDBACK software. Axes x, y and z of the Cartesian reference frame correspond to (0°E, 0°N), (90°E, 0°N), and (90°N), respectively. Covariance matrices are symmetric, thus only upper triangles are tabulated. The finite rotation at 8.132 Ma has been bootstrapped from the noisy data set and interpolated in the noise–mitigated series.

Age [Ma]	Lon. [°E]	Lat. [°N]	Angle [° CCW]	c_{xx}	c_{xy}	c_{xz}	c_{yy} [10^{-8} rad^2]	c_{yz}	c_{zz}
0	32.75	20.26	0.01	27	18	21	11	13	16
0.781	32.74	20.24	0.33	17	9	10	7	8	10
1.778	32.65	20.38	0.74	16	4	2	6	8	11
2.581	32.53	20.54	1.07	28	6	3	9	13	19
3.596	32.34	20.79	1.50	76	27	25	27	35	48
5.235	31.94	21.32	2.13	65	9	-0	21	30	45
6.033	31.74	21.58	2.44	79	12	2	26	36	54
6.733	31.57	21.80	2.72	80	8	-4	26	37	56
8.132	31.24	22.27	3.27	103	11	-3	33	47	70
9.105	31.00	22.61	3.64	120	13	-4	38	54	82
9.786	30.84	22.84	3.90	142	16	-4	45	64	96
11.067	30.54	23.27	4.40	199	22	-4	64	90	134
12.464	30.25	23.70	4.95	261	20	-17	83	119	177
14.607	30.04	24.24	5.81	342	30	-16	110	155	229
15.974	30.13	24.45	6.44	315	37	-2	102	142	208
17.235	30.33	24.59	7.13	214	-9	-51	68	101	157
18.056	30.47	24.66	7.57	233	-30	-85	73	112	180
19.722	30.79	24.79	8.35	580	-125	-293	173	279	466

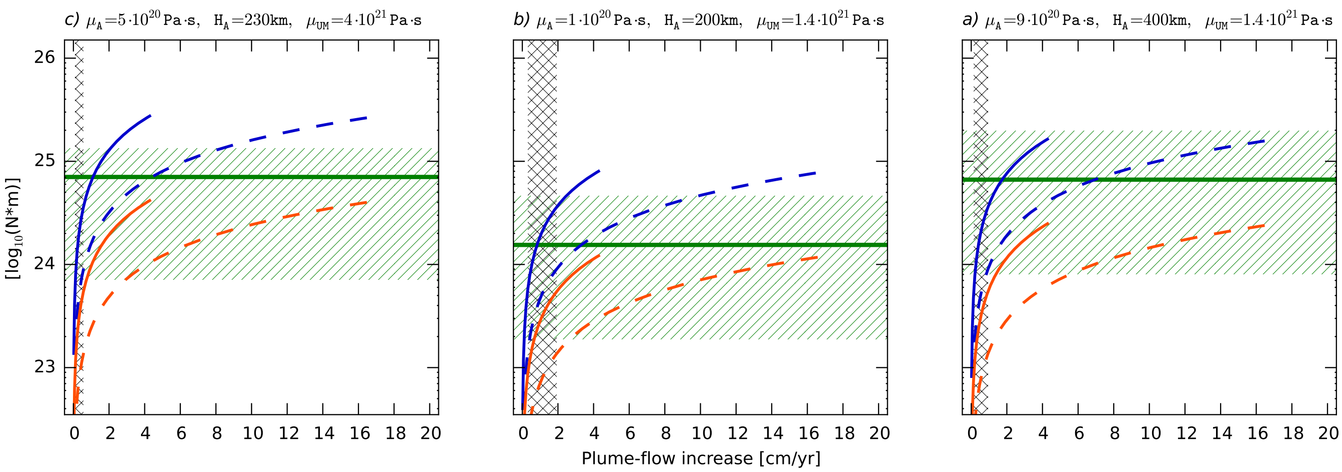

Supplementary Figure 1: **a-c**, Similar to Fig. 4d, for different values of viscosity/thickness of the asthenosphere and viscosity of the lower part of the upper-mantle. Viscosity/thicknesses of the asthenosphere are constrained jointly from glacial rebound data and plate dynamics modelling [2]. Legend and color-coding are similar to those of Fig. 4d.

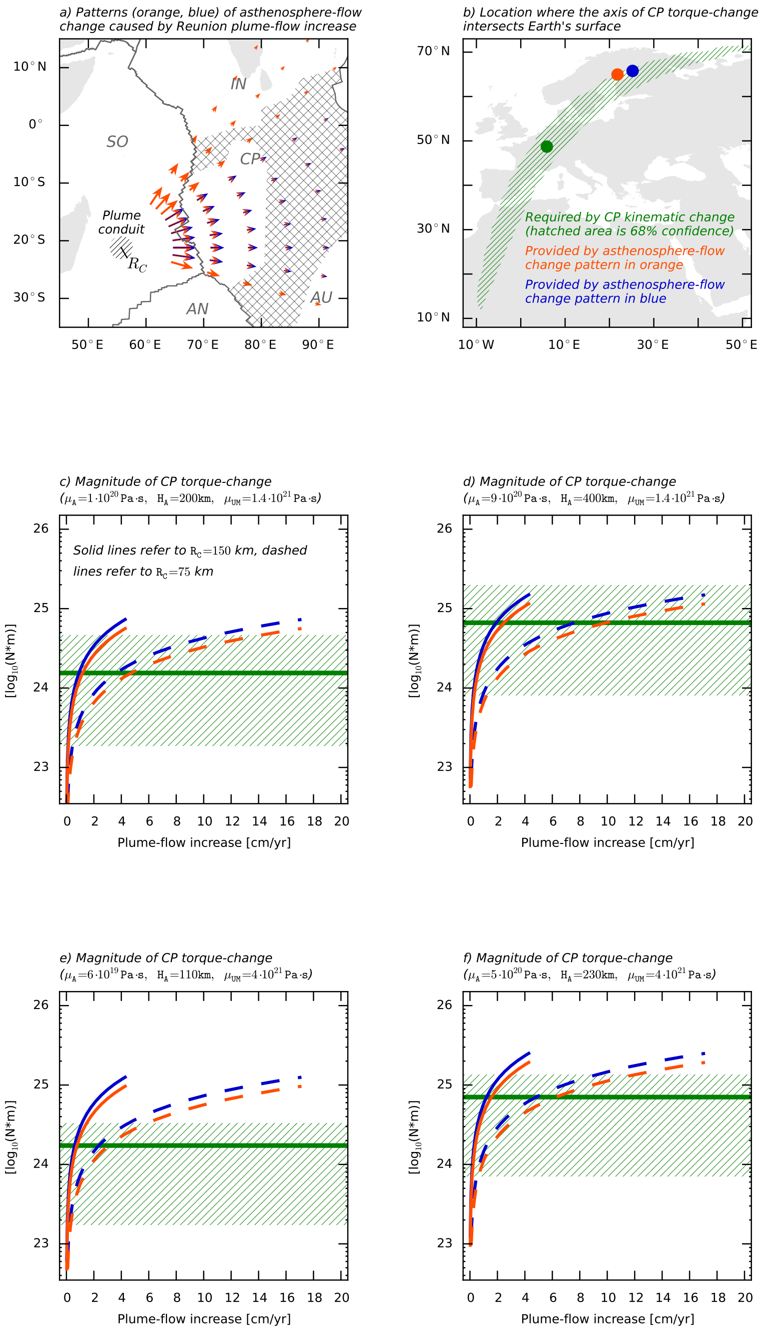

Supplementary Figure 2: **a**, Similar to Fig. 4b, for two different windows of asthenospheric flow-pattern induced by the Reunion plume-flow increase. **b**, Similar to Fig. 4c, for the asthenospheric flow-patterns shown in panel a. **c-f**, Similar to Fig. 4d, for different values of viscosity/thickness of the asthenosphere and viscosity of the lower part of the upper-mantle. Viscosity/thicknesses of the asthenosphere are constrained jointly from glacial rebound data and plate dynamics modelling [2]. Color-coding in similar to panel b. Legend is the same of Fig. 4d.

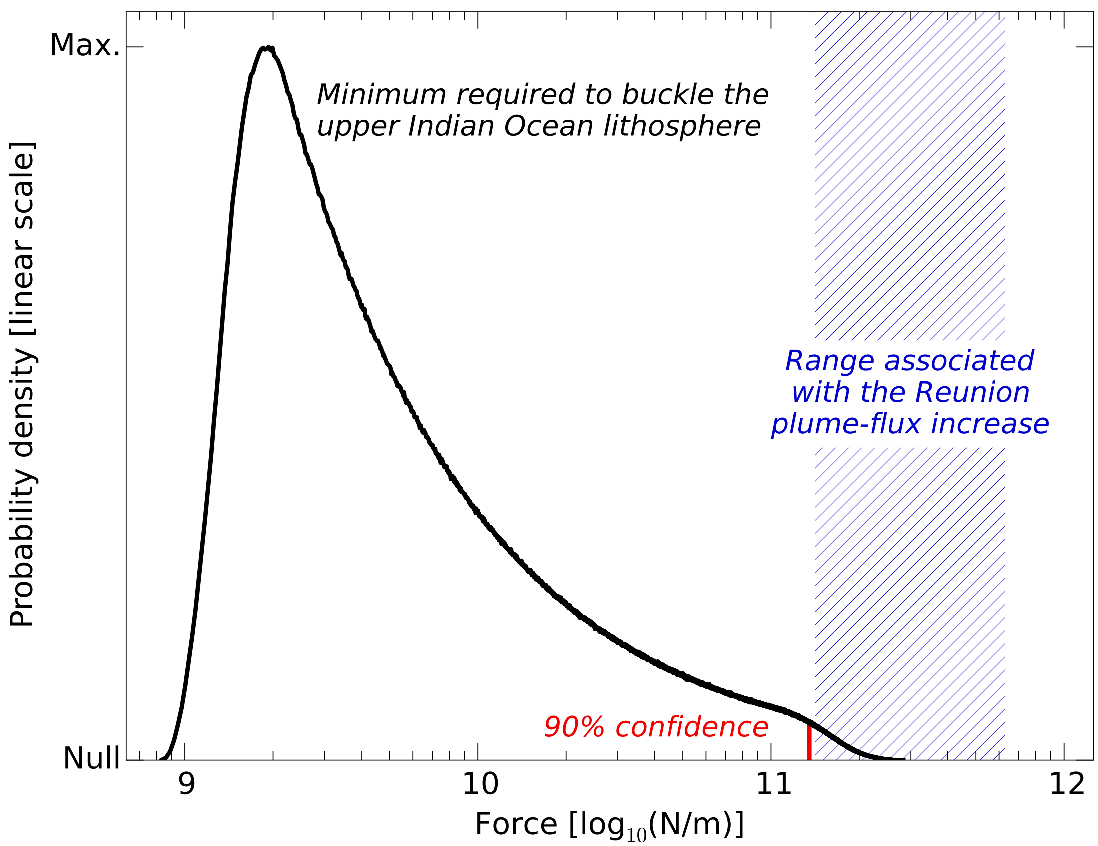

Supplementary Figure 3: Comparison between the probability density distribution (PDD) of the minimum force required to buckle the Indian Ocean lithosphere upper layer (black), and the range of force delivered to the lithosphere by the Reunion plume-flux increase (blue). The analytical expression for the minimum force required to buckle a 2000 to 2500 km wide region is obtained from the elasticity/flexure theory for a plate under horizontal loads (see methods). The PDD is calculated by sampling 10^8 times such an expression, using an equivalent elastic thickness in the range 5 to 25 km, a Young's modulus in the range 0.06 to 0.1 TPa and a Poisson's ratio in the range 0.15 to 0.3. Samples of the parameter values are uniformly distributed within the indicated ranges. The force delivered by the Reunion plume-flux increase is significantly larger than the most probable value of the minimum required for buckling ($\sim 2 \cdot 10^9$ N/m), and - in the most stringent conditions - larger than 90% of the PDD (red).

References

[1] Bull, J. M., DeMets, C., Krishna, K. S., Sanderson, D. J. & Merkouriev, S. Reconciling plate kinematic and seismic estimates of lithospheric convergence in the central Indian Ocean. *Geology* **38**, 307–310 (2010).

[2] Iaffaldano, G. & Lambeck, K. Pacific plate–motion change at the time of the Hawaiian–Emperor bend constrains the viscosity of Earth's asthenosphere. *Geophysical Research Letters* **41**, 3398–3406 (2014).